Calculating the Electron Diffusion Region Aspect Ratio with Magnetic Field Gradients

S.V. Heuer[1], K.J. Genestreti[2], T.K.M. Nakamura[4,5], R.B. Torbert[1,2], J.L. Burch[3], R. Nakamura[4]

[1]University of New Hampshire, Durham, NH, USA
[2]Southwest Research Institute, Durham, NH, USA
[3]Southwest Research Institute, San Antonio, TX, USA
[4]Space Research Institute, Austrian Academy of Sciences, Graz, Austria
[5]Institute of Physics, University of Graz, Graz, 8010, Austria

Key Points:

- A new technique is introduced to calculate the aspect ratio of the electron diffusion region (EDR) with magnetic field gradients.
- The aspect ratio is determined within 20% uncertainty for a particle-in-cell simulation with added MMS-like errors.
- When applied to MMS data the aspect ratio is within uncertainty of the normalized reconnection rate measured during three magnetotail EDRs.

Corresponding author: Steven Heuer, steven.heuer@unh.edu

Abstract

We calculate the aspect ratio of the electron diffusion region (EDR) during symmetric magnetic reconnection using magnetic field gradients measured by the Magnetospheric Multiscale mission (MMS). The technique introduced in this paper is validated using a particle-in-cell (PIC) simulation, compared with the reconnection rate for three MMS-observed magnetotail EDRs, then compared with the EDR aspect ratio predicted by scaling dependencies on asymptotic upstream electron β. For the MMS events, we find that the EDR aspect ratio determined using the magnetic field gradients are within uncertainty of the normalized reconnection rate found by previous studies for three MMS-observed EDRs. Because the magnetic field gradients are velocity-frame independent and typically very well measured by MMS, the technique can be used to obtain the normalized reconnection rate with higher fidelity than established methods.

Plain Language Summary

Magnetic reconnection is a plasma process which occurs throughout the universe. It accelerates and heats nearby particles, and can redistribute energy over vast scales. The rate at which it occurs, the reconnection rate, is one of the most important quantities describing reconnection. Reconnection occurs within an electron-scale region where ions and electrons are decoupled from the magnetic field, known as the electron diffusion region (EDR). Theory and simulations have shown the dimensions of the EDR scale with the reconnection rate. In this paper, we introduce a new method to determine the aspect ratio of the EDR and show that it is the reconnection rate for reconnection events observed by the Magnetospheric Multiscale (MMS) mission. This new method has fewer sources of error than established methods for determining reconnection rate using spacecraft data, and could provide a simpler way of studying the mechanisms which control the reconnection rate.

1 Introduction

1.1 Background

Magnetic reconnection is a fundamental process in plasmas which converts electromagnetic energy stored in magnetic fields to kinetic and thermal particle energy through a change of magnetic field topology (Parker, 1957; Birn & Priest, 2007; Yamada et al., 2010). The field line breaking occurs within a region where the plasma is decoupled from the magnetic field lines, known as the diffusion region. Magnetic reconnection is an inherently multi-scale process (Vasyliunas, 1975). Ions are demagnetized in an ion diffusion region (IDR) at the ion inertial scale, with a smaller electron diffusion region (EDR) embedded within the IDR at the electron inertial scale, where both electrons and ions are demagnetized. Reconnection happens within the EDR, which contains the reconnection X-line (Hesse et al., 1999; Shay et al., 1998).

The EDR is characterized by strong electron non-gyrotropy (Scudder & Daughton, 2008), non-ideal electric field $\vec{E}' = \vec{E} + (\vec{V} \times \vec{B}) \neq 0$, and positive non-ideal energy conversion rate $\vec{J} \cdot \vec{E}' > 0$ (Zenitani et al., 2011). Elongated perpendicular currents in the outflow region have been predicted by simulations (Daughton et al., 2006; Karimabadi et al., 2007) and observed in situ (Phan et al., 2007; Hwang et al., 2017). These electron jets, sometimes known as the outer EDR, have a non-ideal electric field but negative non-ideal energy conversion rate $\vec{J} \cdot \vec{E}' < 0$ (Zenitani et al., 2011).

The rate of reconnection is of order 0.1 in normalized units (Birn et al., 2001; Liu et al., 2022; Cassak et al., 2017). Precise ensemble measurements of reconnection rate are crucial for in situ determination of the parameters controlling the efficiency of reconnection. However, observational measurements of the reconnection rate typically have

compounding sources of error associated with coordinate transformations, velocity frame determination, and uncertainty in the upstream conditions used for normalization (Fuselier & Lewis, 2011; Genestreti et al., 2018). Determining the parameters that control the reconnection rate is a principal goal of NASA's Magnetospheric Multiscale (MMS) mission (Burch et al., 2016).

For quasi-2-dimensional steady-state and incompressible reconnection, a simple geometric argument using conservation of mass, energy, and magnetic flux can be used to show that the reconnection rate scales as the ratio of the EDR dimensions in the outflow and inflow directions (T. Nakamura et al., 2021). The EDR aspect ratio has been found previously using MMS data by directly determining the dimensions of the EDR using spacecraft timing techniques (Torbert et al., 2018; R. Nakamura et al., 2019), techniques which place strict requirements on the EDR encounter geometry. The EDR aspect ratio is an intrinsically normalized quantity independent of velocity frame or upstream conditions, and a general method for determining the EDR aspect ratio would be a measure of the reconnection rate with fewer potential sources of error.

1.2 Theoretical Scaling of the EDR Aspect Ratio

Simulations and theories have shown that the spatial scale of the EDR is determined by the bounce length of electrons trapped within a field reversal (Hesse et al., 1999; Kuznetsova et al., 2000), which has been found analytically (Biskamp & Schindler, 1971). For uniform electron temperature, the aspect ratio δ/l is defined as the ratio of magnetic field gradient terms

$$\frac{\delta}{l} \sim \left[\left(\frac{\partial B_N}{\partial L} \right)^2 / \left(\frac{\partial B_L}{\partial N} \right)^2 \right]^{\frac{1}{4}} \tag{1}$$

where L is the direction of the reconnecting component of the magnetic field, and N is the current sheet normal direction (M, which does not appear in Eq.(1), completes the right-handed LMN coordinate system). R. Nakamura et al. (2019) calculated the EDR dimensions using Eq.(1) by determining the magnetic field gradient from the slope of the magnetic field along the inferred trajectory of MMS through the EDR (the methods used by Torbert et al. (2018) to estimate the dimensions of the EDR also required knowledge of the spacecraft trajectory). These approaches require specific spacecraft trajectory geometries that cross the extent of EDR in the vertical and horizontal directions. However, if the magnetic field gradient terms $\partial B_N/\partial L$ and $\partial B_L/\partial N$ are spatially uniform within the EDR, the aspect ratio can be evaluated with Eq.(1) at any point within the EDR, as local gradients can be determined with multi-point MMS data without any requirements on the trajectory.

Additional scaling relations for the dimensions of the EDR were derived by T. Nakamura et al. (2016) using particle-in-cell (PIC) simulations. The length and width of the EDR L_z and L_x respectively, are described as a function of $\beta_{e\infty}$, the asymptotic upstream electron β. Using these scaling relations, the aspect ratio L_z/L_x is predicted to be

$$\frac{L_z}{L_x} = 0.125 \left(\frac{\beta_{e\infty}}{0.1} \right)^{\frac{1}{8}} \left(1 + 0.15 \left(\frac{\beta_{e\infty}}{0.1} \right)^{-1/2} \right)^{1/2} \tag{2}$$

The aspect ratio L_z/L_x is distinguished from δ/l. While both are descriptions of the EDR aspect ratio, they are defined uniquely. Equation (2) gives a theoretical aspect ratio value for a given set of background plasma conditions which can be compared with experimental values of aspect ratio calculated with Eq.(1). The scaling relations used in Eq.(2) were found for reconnection with an anti-parallel magnetic field configuration and a limited range of upstream background densities, and may require modification for guide field reconnection (Divin et al., 2019; Le et al., 2013). The dimensions in Eq.(1) and Eq.(2) are

also defined differently: Eq.(1) describes the dimensions of the region where electrons have non-gyrotropic orbits, whereas L_z and L_x in Eq.(2) are the dimensions of the region with electron non-gyrotropy and a positive out-of-plane electric field component.

1.3 Outline of this Study

We introduce a general method to calculate the EDR aspect ratio using Eq.(1) and the magnetic field gradient terms measured by MMS. In the following methodology section, we describe how $\nabla\vec{B}$ and $\beta_{e\infty}$ were measured by MMS (section 2.1) and how Eq.(1) is evaluated. In section 3, we use a fully kinetic 2.5-dimensional particle-in-cell (PIC) simulation to quantify the error introduced to Eq.(1) by MMS-like errors in $\nabla\vec{B}$, and the accuracy of the technique as a function of distance from the X-line. In section 4, we use Eq.(2) and the three sets of coordinates described in section 2.2 to calculate δ/l for three magnetotail MMS reconnection events. We compare δ/l with the measured normalized reconnection rate and L_z/L_x. Finally, we summarize and discuss our findings in section 5.

2 Methodology

2.1 MMS Data

The Magnetospheric Multiscale (MMS) Mission is comprised of four spacecraft which orbit Earth in a tetrahedral formation (Burch et al., 2016). This study uses the highest time resolution magnetic field data from the MMS Fluxgate Magnetometer (FGM) (Russell et al., 2016), which was smoothed in time with a Savitzky-Golay filter to reduce noise. The magnetic field data is calibrated to ≤ 0.1nT, with the largest uncertainties being in the spin-axis component of the magnetic field (typically corresponding to B_N in the magnetotail) (Torbert et al., 2016). Particle data used to calculate β was measured by the Fast Plasma Investigation (FPI) (Pollock et al., 2016). For each event, $\beta_{e\infty}$ is calculated by time averaging β_e in the asymptotic upstream region (Table 1). All data was collected during periods when spacecraft separation was on the order of electron inertial length d_e. The linear gradient or curlometer method is used to determine the magnetic field gradient and current within the spacecraft tetrahedron (Chanteur, 1998). For the events studied here, the inter-spacecraft separations were such that the current density was nearly uniform across the MMS tetrahedron, a necessary condition for the linear gradient method.

2.2 Experimental Calculation of EDR Aspect Ratio

Evaluating Eq.(1) for spacecraft data requires determining the L and N directions, which are found in this study using three different methods

1. **Fixed LMN**: here we use a fixed (time independent) *LMN* coordinate system to obtain the EDR aspect ratio from Eq.(1). The fixed *LMN* system is determined with a hybrid approach (Genestreti et al., 2018; Denton et al., 2018): minimum variance analysis of the electron bulk velocity (MVA-V_e) or magnetic field (MVA-B) are used to determine L (Sonnerup & Scheible, 2000). MVA-B is used when the EDR is crossed in the normal direction. MVA-V_e is used when the EDR is crossed laterally, from one outflow to the other. The N direction was defined using the maximum directional derivative of the magnetic field (MDD-B) technique (Shi et al., 2005) which determines coordinates as the eigenvectors of the matrix $(\nabla\vec{B})(\nabla\vec{B})^T$. The M vector $N \times L/|N \times L|$ completes the right-handed coordinate system.
2. **MDD-B LMN**: here we used the terms of $\nabla\vec{B}$ in the time-varying *LMN* coordinates from MDD-B to evaluate Eq.(1) and determine the aspect ratio δ/l.

3. **MDD-B Eigenvalue Ratio**: similar to the MDD-B LMN method, we evaluated Eq.(1) with time-varying *LMN* coordinates from MDD-B, but with three additional a priori assumptions: that the EDR is quasi-2-dimensional, inflow-symmetric, and anti-parallel. Under these assumptions, the only non-vanishing terms of $\nabla\vec{B}$ at the current sheet center are $\partial B_L/\partial N = \sqrt{\lambda_N}$ and $\partial B_N/\partial L = \sqrt{\lambda_L}$, where λ_N and λ_L are the maximum and intermediate eigenvalues of $(\nabla\vec{B})(\nabla\vec{B})^T$. Thus the aspect ratio is $\delta/l = (\lambda_L/\lambda_N)^{1/4}$.

The three techniques above each yield time-dependent functions δ/l. Single, nominal values and approximate uncertainties for δ/l are selected for each as the average of the three over an 0.1 second interval around the current sheet (see section 3). The uncertainty is found by taking the standard deviation of the data points over the same interval.

3 Quantifying Errors in the Aspect Ratio with a Simulation

The different sources of error in the calculation of the δ/l are characterized using a PIC simulation of the 11 July 2017 magnetotail reconnection event observed by MMS which has been found to be extremely consistent with observations (T. Nakamura et al., 2018). The sources of error considered here are how the absolute error depends on distance from reconnection X-line, and the error introduced from MMS-like uncertainties in magnetic field. In this simulation, the coordinate system is known exactly so there are none of the errors introduced when transforming to an *LMN* coordinate system.

The EDR in the simulation is defined as the region surrounding the X-line where the out-of-plane component of the electron frame electric field is positive, $E'_M > 0$. The aspect ratio of the central EDR for this simulation is calculated to be 0.24. An upper-bound estimate for the characteristic magnetic field measurement error for MMS of 0.1 nT was added to $\partial B_N/\partial L$ during the aspect ratio calculation and normalized by the average spacecraft separation for 11 July EDR encounter $\Delta R_{SC} = 0.58 d_e$ (Figure 1b and 1c). The uncertainty for a nominal MMS-like error of 0.01 nT was also calculated, but no substantial difference from the no error case was observed with uncertainty below 10% within the central EDR (not pictured).

At the center of the current sheet, aspect ratio from the Fixed LMN and MDD-B Eigenvalue Ratio methods are both within 20% of the actual value. In the no error case, the uncertainties in both methods are below 10% within the entire central EDR. As expected, the accuracy of each technique depends on the relative position of the MMS tetrahedron within the reconnection region. The aspect ratio determined with the Fixed LMN method is more accurate along the separatrices, compared with the aspect ratio from the MDD-B Eigenvalue Ratio method (Figure 1c and 1d). This is expected, as the assumptions made about reconnection geometry for the MDD-B Eigenvalue Ratio are only accurate where the out-of-plane gradient is small, such as the central EDR and along the current sheet center (see section 2.2). When these conditions are satisfied, the MDD-B Eigenvalue Ratio method can be more accurate than the Fixed LMN method. The 1-dimensional cuts of the aspect ratio along the reconstructed MMS trajectory for 11 July (Figure 1e and 1f) show that both Fixed LMN and MDD-B Eigenvalue Ratio derived aspect ratios should be within 20% of the EDR aspect ratio for nominal MMS-like errors at the center of the current sheet, which is observed in the MMS data (Figure 3c).

The low uncertainty close to the center of the current sheet shows that the magnetic field gradient can be used to accurately measure the aspect ratio of the EDR within the central EDR, even with upper-bound MMS-like magnetic field errors. Additionally, Figure 2 also suggests that measurements beyond the central EDR may also accurately measure the EDR aspect ratio. However, further work is necessary to determine whether the aspect ratio of the outer EDR generally corresponds to that of the central EDR.

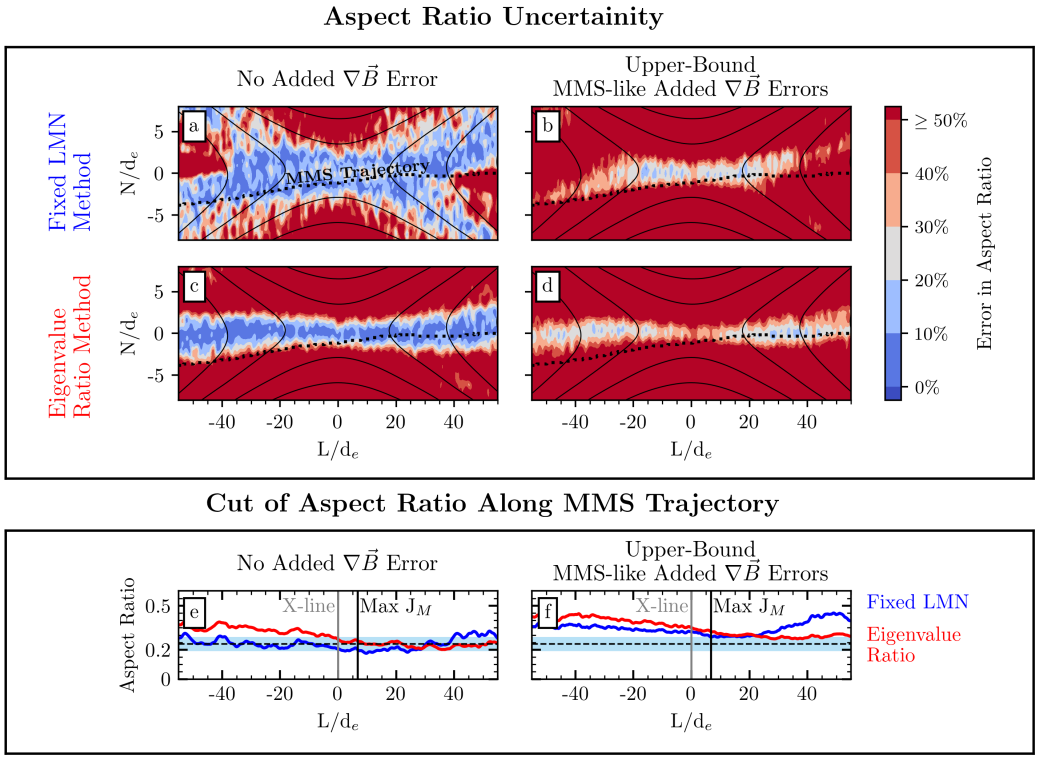

Figure 1. Panels (a), (b) and (c), (d) show the uncertainty in the aspect ratio determined using the Fixed *LMN* and the MDD-B Eigenvalue Ratio techniques and magnetic field gradients from the PIC simulation of the 11 July 2017 event. Panels (a) and (c) are displayed with no error, while (b) and (d) have MMS-like errors added to $\nabla\vec{B}$ before calculating the aspect ratio. Panels (e) and (f) show a 1-dimensional cut of the along the reconstructed MMS trajectory, compared with the aspect ratio of 0.24 and the 20% uncertainty indicated with blue shading. The X-line and Max J_M are defined as the reversal of B_N and maximum J_M along the reconstructed trajectory, respectively.

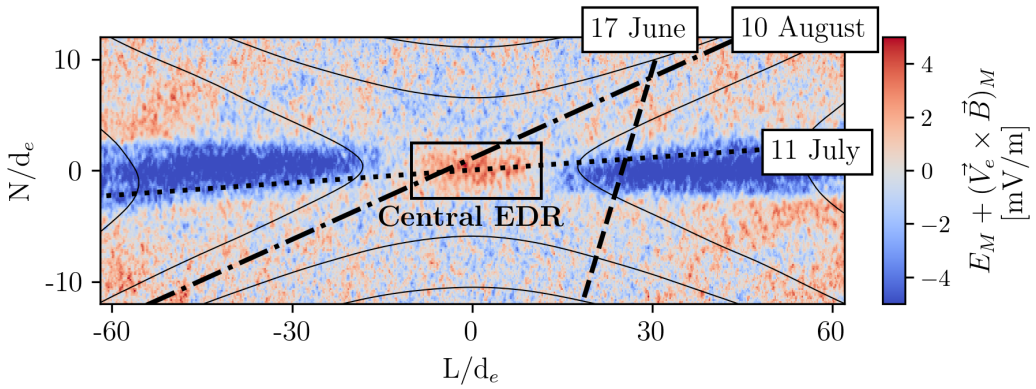

Figure 2. Diagram showing the approximate trajectories for the three events used in this study relative to the central EDR determined using the reconnection electric field E'_M from the 11 July PIC simulation.

Table 1. Calculated parameters for the three EDR encounters. L_z/L_x is the aspect ratio calculated using Eq.(2), and δ/l, the average aspect ratio at the center of the current sheet.

Event	δ/l	Reconnection Rate	L_z/L_x	Upstream Interval for L_z/L_x
11 July 2017	0.210 ± 0.041	0.180 ± 0.035^a	0.146 ± 0.039	22:31-22:31:50
10 August 2017	0.202 ± 0.054	0.190 ± 0.040^b	0.151 ± 0.019	12:19:17-12:19:19
17 June 2017	0.119 ± 0.077	0.077 ± 0.050^c	0.145 ± 0.010	20:24:45-20:25

^{a}(Genestreti et al., 2018) ^{b}(Li et al., 2019) ^{c}(Farrugia et al., 2021)

3.1 EDR Aspect Ratio with Data from MMS

Next we apply the techniques described in section 2.2 to MMS observations for three symmetric magnetotail reconnection events: the previously discussed 11 July 2017 event, 10 August 2017 (Zhou et al., 2019), and 17 June 2017 (Farrugia et al., 2021). The trajectories of MMS through each of the three EDRs differed (see Figure 2), but all three passed through regions where the PIC simulation analysis predicts the aspect ratio can be determined within 20% uncertainty.

During the 11 July 2017 EDR encounter, MMS crossed the EDR along the magnetotail current sheet, moving predominantly in the L-direction, and the small B_L indicates it spent a significant of time in the current sheet (Figure 3a) where the current density is largest (Figure 3b). This is consistent with the spatial region where the simulation tells us the uncertainty in δ/l is smallest (Figure 1). For this event, we find that the EDR aspect ratio calculated by R. Nakamura et al. (2019) and normalized reconnection rate from Genestreti et al. (2018) are both within the error bars of δ/l (Figure 3c). The 19% uncertainty in δ/l is comparable to the 20% upper-bound uncertainty estimated from the PIC simulation results in section 3. While the reconnection rate uncertainty of 0.035 found by Genestreti et al. (2018) is smaller than the δ/l upper-bound uncertainty, the 11 July EDR is an ideal case which permitted errors being characterized and minimized with a detailed study. Additionally, the reconnection rate error calculated by Genestreti et al. (2018) does not account for uncertainties in the upstream conditions used for normalization.

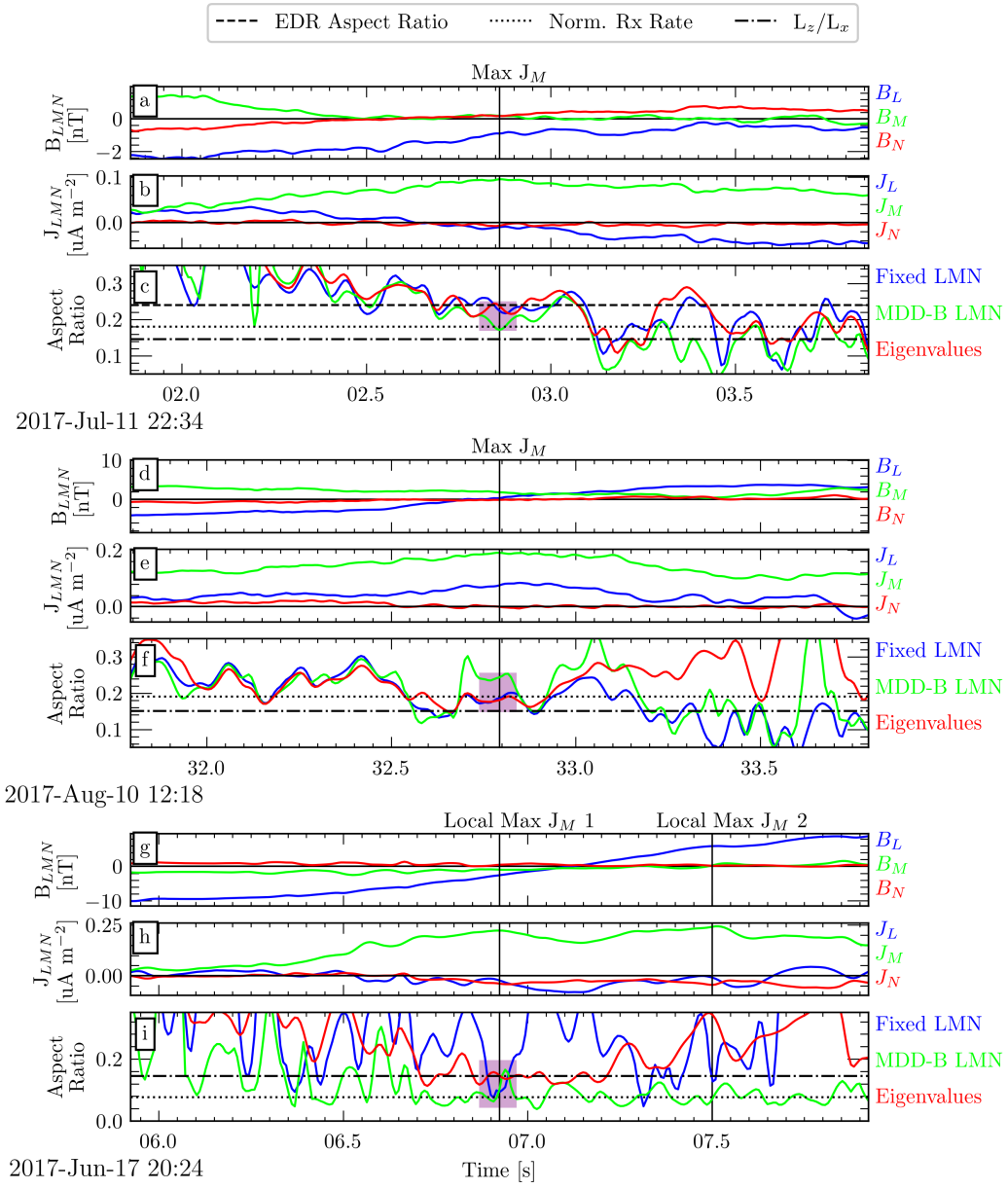

Figure 3. Summary of the 11 July 2017, 10 August 2017, and 17 June 2017 EDR encounters. Panels (a), (d), and (g) show the 4-point average magnetic field in *LMN* coordinates B_{LMN}. Panels (b), (e), and (h) show the current density in *LMN* coordinates J_{LMN}. Panels (c), (f), and (i) show the aspect ratio determined using the Fixed LMN, the MDD-B LMN, and the MDD-B Eigenvalue methods (see Table 1). Purple shading indicates the uncertainty in δ/l over an 0.1 second interval around maximum J_M.

On 10 August MMS crossed the EDR obliquely (Zhou et al., 2019), and the magnitude of the aspect ratio determined using the Fixed LMN and MDD-B Eigenvalue Ratio methods are close at the center of the current sheet, while the MDD-B LMN derived aspect ratio is larger (Figure 3f). δ/l is within the error bars of the normalized reconnection rate determined by Li et al. (2019) for 10 August (Table 1). The trajectory for the 17 June encounter was different from the 11 July and 10 August central EDR encounters, in that on 17 June MMS crossed the outer EDR (Farrugia et al., 2021). Additionally, Figure 3h shows the EDR had a double-peaked current structure labeled "Local Max J_M 1 and 2." The aspect ratio δ/l at the first peak is within the error bars of the normalized reconnection calculated by Farrugia et al. (2021) for the 17 June EDR.

Next we compare the δ/l with the predicted EDR aspect ratio by calculating $\beta_{e\infty}$ for each event and evaluating Eq.(2). The upstream intervals and L_z/L_x for each event are summarized in Table 1. The nominal normalized reconnection rate from Genestreti et al. (2018) for 11 July is within the error bars of L_z/L_x, but not the aspect ratio $0.240\pm$ 0.071 from R. Nakamura et al. (2019). For 10 August, L_z/L_x is outside of the error bars for both δ/l and the normalized reconnection rate from Li et al. (2019). The 17 June event, where MMS did not encounter the central EDR, was the only event where L_z/L_x is larger than the reconnection rate and δ/l, but still outside the error bars.

4 Summary and Conclusions

We have introduced a new technique for calculating the aspect ratio of the EDR using the magnetic field gradient, with the effect of MMS-like errors in the magnetic field quantified using a PIC simulation. The aspect ratio of the EDR calculated with the magnetic field gradient has an error below 20% within the central EDR even for the upper-bound MMS magnetic field errors. We used MMS data to calculate the aspect ratio δ/l for three magnetotail EDR encounters and showed that it is within error bars of the measured normalized reconnection rate for all three events. All values of δ/l calculated using the methods introduced in this paper are within the range 0.1-0.2, which is expected from past studies of fast reconnection (Liu et al., 2017; Liu et al., 2022).

During the first event studied, 11 July 2017, MMS passed through the EDR laterally, spending an extended period of time along the current sheet. As predicted by the PIC simulation in section 2, we find δ/l measured at the center of the current sheet is within 20% of the EDR aspect ratio and normalized reconnection rate. During the second event studied, 10 August 2017, MMS cut through the central EDR along the separatrices. While MMS spent less time in the current sheet during the 10 August EDR encounter compared to 11 July, δ/l is within 20% of the normalized reconnection rate localized in the center of the current sheet. During the third event studied, 17 June 2017, MMS did not encounter the central EDR, but crossed the extended electron outflow jets downstream, with a bifurcated structure in the out-of-plane current density. Despite not traversing the central EDR, the normalized reconnection rate was within the uncertainty in δ/l at the first current peak. This is consistent with the PIC simulation error analysis that suggested the aspect ratio measured in the outer EDR corresponds to the aspect ratio of the central EDR, which is a result meriting further investigation. The accuracy of the Fixed LMN, MDD-B LMN, and MDD-B Eigenvalue Ratio techniques may depend on the background plasma conditions where reconnection occurs (e.g. guide field strength, which modifies the electron meandering motions and the Hall current system). A more detailed parameter analysis (beyond the single simulation analyzed in section 3) is required to determine the relative accuracy of each technique in a meaningful way.

The aspect ratio L_z/L_x determined using Eq.(2) and the asymptotic upstream electron $\beta_{e\infty}$ is found to be consistently below the normalized reconnection rate and δ/l. Equation (2) was determined for anti-parallel reconnection, and all three events had a small guide field. Another potential explanation is difference in EDR definition. The dimen-

sions L_z and L_x are determined as boundaries of the region with non-gyrotropic electrons, and the outer EDR has been observed to exhibit some electron non-gyrotropy. Since the aspect ratio is inversely proportional to L_x, an elongated EDR would decrease the aspect ratio. While the magnitude of L_z/L_x is less than δ/l, we are unable to determine whether they scale the same with available data, but the relative scaling of δ/l and L_z/L_x may be tested using any future magnetotail encounters with higher or lower values of $\beta_{e\infty}$.

Established methods for estimating the normalized reconnection rate in situ require normalization by upstream quantities with large uncertainties, and place constraints on spacecraft trajectory. We have shown that the EDR aspect ratio can be used as a measure of reconnection rate for symmetric 2-dimensional laminar reconnection in the magnetotail. Since the technique presented in this paper for determining the EDR aspect ratio using $\nabla\vec{B}$ and Eq.(1) is a normalized quantity that can be measured anywhere within the central EDR, it can be used to estimate the normalized reconnection rate independent of spacecraft trajectory through the EDR and with fewer sources of error than established methods.

Further work is necessary determine the accuracy of Eq.(1) when one or more of the assumptions are violated, such as during asymmetric or guide field reconnection. The multi-spacecraft $\nabla\vec{B}$ reconstruction technique used in this study assumed that the current density within the MMS tetrahedron was spatially uniform. While this assumption was shown to be valid for the three EDRs studied in this paper, a higher-order gradient reconstruction method (Torbert et al., 2020; Denton et al., 2020) may be necessary for EDRs with smaller characteristic length scales, such as at the magnetopause.

Appendix A PIC Simulation Setup

In this paper, we analyzed a 2.5-dimensional simulation of the 11 July 2017 MMS event performed by T. Nakamura et al. (2018) using the fully kinetic particle-in-cell code VPIC (Bowers et al., 2008, 2009). The simulation initial conditions were based on MMS observations of the plasma sheet and lobes (see T. Nakamura et al. (2018) for full description of simulation parameters). The system size was $120d_{i0} \times 40d_{i0}$, where d_{i0} is the ion inertial length in the initial current sheet, with a total of $1.4{\times}10^{11}$ super particles and an ion-to-electron mass ratio of 400. The initial current sheet was symmetric with a guide field of 0.03. At the time shown in Figure 1 (50 ion cyclotron periods after simulation start), the reconnection rate had developed to a steady state. The irregular cut shown in Figure 1 through the simulated EDR was selected to match the MMS trajectory by a best fit of B_L.

Data Availability Statement

The MMS FIELDS and FPI data used in this study are publicly available from the Science Data Center (SDC) at https://lasp.colorado.edu/mms/sdc/public/about/browse. Routines from the pySPEDAS and pyTplot libraries used to process the MMS data analyzed in this paper (Grimes et al., 2019) are freely available at https://github.com/spedas/pyspedas.

Acknowledgments
S.V.H., K.J.G., and R.B.T. were supported by NASA's MMS FIELDS Grant NNG04EB99C. T.K.M.N. was supported by the Austrian Research Fund (FWF): P32175-N27. For the simulation analyzed in this paper, we acknowledge PRACE for awarding us access to MareNostrum at Barcelona Supercomputing Center (BSC), Spain.

References

Birn, J., Drake, J. F., Shay, M. A., Rogers, B. N., Denton, R. E., Hesse, M., ... Pritchett, P. L. (2001). Geospace environmental modeling (gem) magnetic reconnection challenge. *Journal of Geophysical Research: Space Physics*, *106*(A3), 3715-3719. doi: https://doi.org/10.1029/1999JA900449

Birn, J., & Priest, E. R. (2007). *Reconnection of magnetic fields : magnetohydrodynamics and collisionless theory and observations.*

Biskamp, ., D, & Schindler, K. (1971). Instability of two-dimensional collisionless plasmas with neutral points. *Plasma Physics*, *13*, 1013-2026.

Bowers, K. J., Albright, B. J., Yin, L., Bergen, B., & Kwan, T. J. T. (2008, May). Ultrahigh performance three-dimensional electromagnetic relativistic kinetic plasma simulationa). *Physics of Plasmas*, *15*(5), 055703. doi: 10.1063/1.2840133

Bowers, K. J., Albright, B. J., Yin, L., Daughton, W., Roytershteyn, V., Bergen, B., & Kwan, T. J. T. (2009, July). Advances in petascale kinetic plasma simulation with VPIC and Roadrunner. In *Journal of physics conference series* (Vol. 180, p. 012055). doi: 10.1088/1742-6596/180/1/012055

Burch, J. L., Moore, T. E., Torbert, R. B., & Giles, B. L. (2016, March). Magnetospheric Multiscale Overview and Science Objectives. *Space Science Reviews*, *199*(1-4), 5-21. doi: 10.1007/s11214-015-0164-9

Burch, J. L., Torbert, R. B., Phan, T. D., Chen, L.-J., Moore, T. E., Ergun, R. E., ... Chandler, M. (2016). Electron-scale measurements of magnetic reconnection in space. *Science*, *352*(6290), aaf2939. doi: 10.1126/science.aaf2939

Cassak, P. A., Liu, Y.-H., & Shay, M. A. (2017). A review of the 0.1 reconnection rate problem. *Journal of Plasma Physics*, *83*(5), 715830501. doi: 10.1017/S0022377817000666

Chanteur, G. (1998). Spatial interpolation for four spacecraft: Theory. In G. Paschmann & P. Daly (Eds.), *Analysis Methods for Multi-Spacecraft Data.* The International Space Science Institute, Bern, Switzerland.

Daughton, W., Scudder, J., & Karimabadi, H. (2006). Fully kinetic simulations of undriven magnetic reconnection with open boundary conditions. *Physics of Plasmas*, *13*(7), 072101. doi: 10.1063/1.2218817

Denton, R. E., Sonnerup, B. U. Ö., Russell, C. T., Hasegawa, H., Phan, T. D., Strangeway, R. J., ... Vines, S. K. (2018, March). Determining L-M-N Current Sheet Coordinates at the Magnetopause From Magnetospheric Multiscale Data. *Journal of Geophysical Research (Space Physics)*, *123*(3), 2274-2295. doi: 10.1002/2017JA024619

Denton, R. E., Torbert, R. B., Hasegawa, H., Dors, I., Genestreti, K. J., Argall, M. R., ... Fischer, D. (2020). Polynomial reconstruction of the reconnection magnetic field observed by multiple spacecraft. *Journal of Geophysical Research: Space Physics*, *125*(2), e2019JA027481. (e2019JA027481 10.1029/2019JA027481) doi: https://doi.org/10.1029/2019JA027481

Divin, A., Semenov, V., Zaitsev, I., Korovinskiy, D., Deca, J., Lapenta, G., ... Markidis, S. (2019, October). Inner and outer electron diffusion region of antiparallel collisionless reconnection: Density dependence. *Physics of Plasmas*, *26*(10), 102305. doi: 10.1063/1.5109368

Farrugia, C. J., Rogers, A. J., Torbert, R. B., Genestreti, K. J., Nakamura, T. K. M., Lavraud, B., ... Dors, I. (2021, March). An Encounter With the Ion and Electron Diffusion Regions at a Flapping and Twisted Tail Current Sheet. *Journal of Geophysical Research (Space Physics)*, *126*(3), e28903. doi: 10.1029/2020JA028903

Fuselier, S. A., & Lewis, W. S. (2011). Properties of near-earth magnetic reconnection from in-situ observations. *Space Science Reviews*, *160*(1), 95. Retrieved from `https://doi.org/10.1007/s11214-011-9820-x` doi: 10.1007/s11214-011-9820-x

Genestreti, K. J., Nakamura, T., Nakamura, R., Denton, R. E., Torbert, R. B., Burch, J. L., ... Russell, C. T. (2018). How accurately can we measure the reconnection rate em for the mms diffusion region event of 11 july 2017? *Journal of Geophysical Research: Space Physics*, *123*(11), 9130-9149. doi: https://doi.org/10.1029/2018JA025711

Grimes, E. W., Hatzigeorgiu, N., Lewis, J. W., Russell, C., McTiernan, J. M., Drozdov, A., & Angelopoulos, V. (2019, December). pySPEDAS: Space Physics Environment Data Analysis Software in Python. In *Agu fall meeting abstracts* (Vol. 2019, p. SH41C-3313).

Hesse, M., Schindler, K., Birn, J., & Kuznetsova, M. (1999). The diffusion region in collisionless magnetic reconnection. *Physics of Plasmas*, *6*(5), 1781-1795. doi: 10.1063/1.873436

Hwang, K. J., Sibeck, D. G., Choi, E., Chen, L. J., Ergun, R. E., Khotyaintsev, Y., ... Torbert, R. B. (2017, March). Magnetospheric Multiscale mission observations of the outer electron diffusion region. *Geophysical Research Letters*, *44*(5), 2049-2059. doi: 10.1002/2017GL072830

Karimabadi, H., Daughton, W., & Scudder, J. (2007, July). Multi-scale structure of the electron diffusion region. *Geophysical Research Letters*, *34*(13), L13104. doi: 10.1029/2007GL030306

Kuznetsova, M. M., Hesse, M., & Winske, D. (2000). Toward a transport model of collisionless magnetic reconnection. *Journal of Geophysical Research: Space Physics*, *105*(A4), 7601-7616. Retrieved from `https://agupubs.onlinelibrary.wiley.com/doi/abs/10.1029/1999JA900396` doi: https://doi.org/10.1029/1999JA900396

Le, A., Egedal, J., Ohia, O., Daughton, W., Karimabadi, H., & Lukin, V. S. (2013, March). Regimes of the Electron Diffusion Region in Magnetic Reconnection. *Phys. Rev. Lett.*, *110*(13), 135004. doi: 10.1103/PhysRevLett.110.135004

Li, X., Wang, R., Lu, Q., Hwang, K.-J., Zong, Q., Russell, C. T., & Wang, S. (2019). Observation of nongyrotropic electron distribution across the electron diffusion region in the magnetotail reconnection. *Geophysical Research Letters*, *46*(24), 14263-14273. Retrieved from `https://agupubs.onlinelibrary.wiley.com/doi/abs/10.1029/2019GL085014` doi: https://doi.org/10.1029/2019GL085014

Liu, Y.-H., Cassak, P., Li, X., Hesse, M., Lin, S.-C., & Genestreti, K. (2022, December). First-principles theory of the rate of magnetic reconnection in magnetospheric and solar plasmas. *Communications Physics*, *5*(1), 97. doi: 10.1038/s42005-022-00854-x

Liu, Y.-H., Hesse, M., Guo, F., Daughton, W., Li, H., Cassak, P. A., & Shay, M. A. (2017, Feb). Why does steady-state magnetic reconnection have a maximum local rate of order 0.1? *Phys. Rev. Lett.*, *118*, 085101. Retrieved from `https://link.aps.org/doi/10.1103/PhysRevLett.118.085101` doi: 10.1103/PhysRevLett.118.085101

Nakamura, R., Genestreti, K. J., Nakamura, T., Baumjohann, W., Varsani, A., Nagai, T., ... Torbert, R. B. (2019). Structure of the current sheet in the 11 july 2017 electron diffusion region event. *Journal of Geophysical Research: Space Physics*, *124*(2), 1173-1186. doi: https://doi.org/10.1029/2018JA026028

Nakamura, T., Genestreti, K. J., Liu, Y.-H., Nakamura, R., Teh, W.-L., Hasegawa, H., ... Giles, B. L. (2018). Measurement of the magnetic reconnection rate in the earth's magnetotail. *Journal of Geophysical Research: Space Physics*, *123*(11), 9150-9168. doi: https://doi.org/10.1029/2018JA025713

Nakamura, T., Hasegawa, H., Genestreti, K. J., Denton, R. E., Phan, T. D., Stawarz, J. E., ... Nystrom, W. D. (2021). Fast cross-scale energy transfer during turbulent magnetic reconnection. *Geophysical Research Letters*, *48*(13), e2021GL093524. Retrieved from `https://agupubs.onlinelibrary.wiley.com/doi/abs/10.1029/2021GL093524` (e2021GL093524 2021GL093524) doi:

https://doi.org/10.1029/2021GL093524

Nakamura, T., Nakamura, R., & Haseagwa, H. (2016). Spatial dimensions of the electron diffusion region in anti-parallel magnetic reconnection. *Annales Geophysicae*, *34*(3), 357–367. doi: 10.5194/angeo-34-357-2016

Parker, E. N. (1957, December). Sweet's Mechanism for Merging Magnetic Fields in Conducting Fluids. *Journal of Geophysical Research*, *62*(4), 509-520. doi: 10.1029/JZ062i004p00509

Phan, T. D., Drake, J. F., Shay, M. A., Mozer, F. S., & Eastwood, J. P. (2007, December). Evidence for an Elongated (¿60 Ion Skin Depths) Electron Diffusion Region during Fast Magnetic Reconnection. *Phys. Rev. Lett.*, *99*(25), 255002. doi: 10.1103/PhysRevLett.99.255002

Pollock, C., Moore, T., Jacques, A., Burch, J., Gliese, U., Saito, Y., ... Zeuch, M. (2016, March). Fast Plasma Investigation for Magnetospheric Multiscale. *Space Science Reviews*, *199*(1-4), 331-406. doi: 10.1007/s11214-016-0245-4

Russell, C. T., Anderson, B. J., Baumjohann, W., Bromund, K. R., Dearborn, D., Fischer, D., ... Richter, I. (2016, March). The Magnetospheric Multiscale Magnetometers. *Space Science Reviews*, *199*(1-4), 189-256. doi: 10.1007/s11214-014-0057-3

Scudder, J., & Daughton, W. (2008, June). "Illuminating" electron diffusion regions of collisionless magnetic reconnection using electron agyrotropy. *Journal of Geophysical Research (Space Physics)*, *113*(A6), A06222. doi: 10.1029/2008JA013035

Shay, M. A., Drake, J. F., Denton, R. E., & Biskamp, D. (1998). Structure of the dissipation region during collisionless magnetic reconnection. *Journal of Geophysical Research: Space Physics*, *103*(A5), 9165-9176. doi: https://doi.org/10.1029/97JA03528

Shi, Q. Q., Shen, C., Pu, Z. Y., Dunlop, M. W., Zong, Q. G., Zhang, H., ... Balogh, A. (2005, June). Dimensional analysis of observed structures using multipoint magnetic field measurements: Application to Cluster. *Geophysical Research Letters*, *32*(12), L12105. doi: 10.1029/2005GL022454

Sonnerup, B., & Scheible, M. (2000). Minimum and maximum variance analysis. In G. Paschmann & P. Daly (Eds.), *Analysis Methods for Multi-spacecraft Data* (p. 183-22). The International Space Science Institute, Bern, Switzerland.

Torbert, R. B., Burch, J. L., Phan, T. D., Hesse, M., Argall, M. R., Shuster, J., ... Saito, Y. (2018). Electron-scale dynamics of the diffusion region during symmetric magnetic reconnection in space. *Science*, *362*(6421), 1391-1395. doi: 10.1126/science.aat2998

Torbert, R. B., Dors, I., Argall, M. R., Genestreti, K. J., Burch, J. L., Farrugia, C. J., ... Strangeway, R. J. (2020). A new method of 3-d magnetic field reconstruction. *Geophysical Research Letters*, *47*(3), e2019GL085542. Retrieved from `https://agupubs.onlinelibrary.wiley.com/doi/abs/10.1029/2019GL085542` (e2019GL085542 2019GL085542) doi: https://doi.org/10.1029/2019GL085542

Torbert, R. B., Russell, C. T., Magnes, W., Ergun, R. E., Lindqvist, P. A., Le Contel, O., ... Lappalainen, K. (2016, March). The FIELDS Instrument Suite on MMS: Scientific Objectives, Measurements, and Data Products. *Space Science Reviews*, *199*(1-4), 105-135. doi: 10.1007/s11214-014-0109-8

Vasyliunas, V. M. (1975, February). Theoretical models of magnetic field line merging, 1. *Reviews of Geophysics and Space Physics*, *13*, 303-336. doi: 10.1029/RG013i001p00303

Yamada, M., Kulsrud, R., & Ji, H. (2010, Mar). Magnetic reconnection. *Rev. Mod. Phys.*, *82*, 603–664. doi: 10.1103/RevModPhys.82.603

Zenitani, S., Hesse, M., Klimas, A., & Kuznetsova, M. (2011, May). New measure of the dissipation region in collisionless magnetic reconnection. *Phys. Rev. Lett.*, *106*, 195003.

Zhou, M., Deng, X. H., Zhong, Z. H., Pang, Y., Tang, R. X., El-Alaoui, M., ... Lindqvist, P.-A. (2019, jan). Observations of an electron diffusion region in symmetric reconnection with weak guide field. *The Astrophysical Journal*, *870*(1), 34. doi: 10.3847/1538-4357/aaf16f

Figure 1.

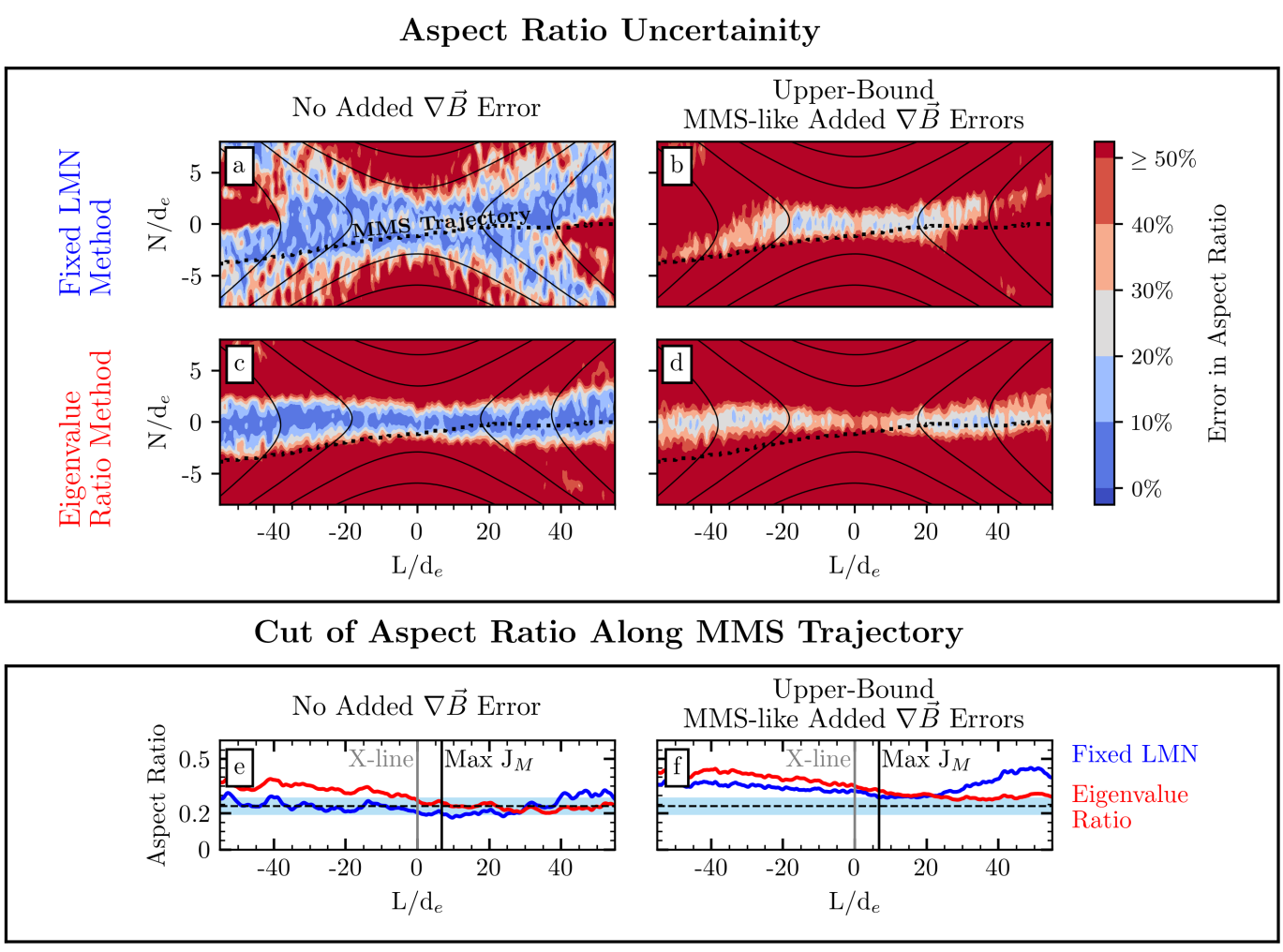
Aspect Ratio Uncertainity
No Added $\nabla\vec{B}$ Error
Upper-Bound
MMS-like Added $\nabla\vec{B}$ Errors
Fixed LMN
Method
Eigenvalue
Ratio Method
a
b
c
d
MMS Trajectory
N/d$_e$
L/d$_e$
≥ 50%
40%
30%
20%
10%
0%
Error in Aspect Ratio
Cut of Aspect Ratio Along MMS Trajectory
Aspect Ratio
e
f
X-line
Max J$_M$
Fixed LMN
Eigenvalue
Ratio

Figure 2.

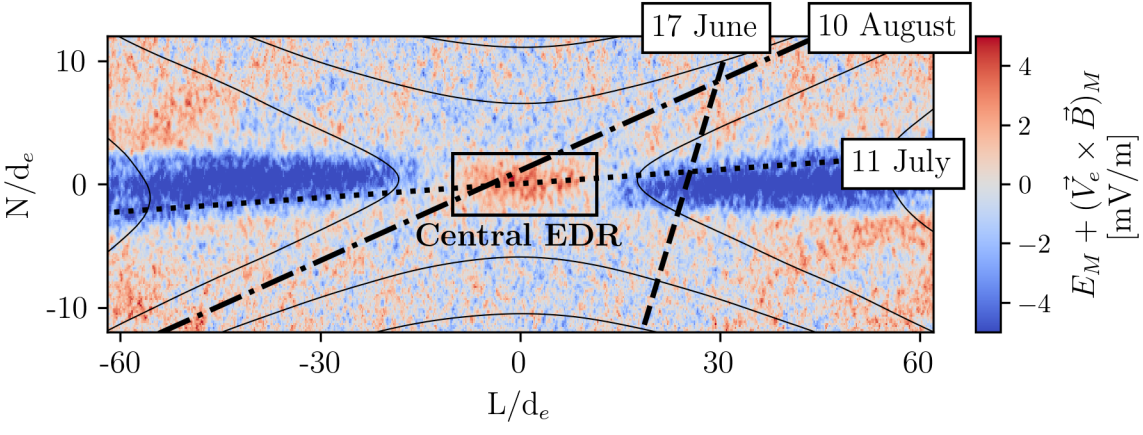
17 June
10 August
11 July
Central EDR
10
0
-10
N/d$_e$
-60
-30
0
30
60
L/d$_e$
4
2
0
−2
−4
$E_M + (\vec{V}_e \times \vec{B})_M$
[mV/m]

Figure 3.

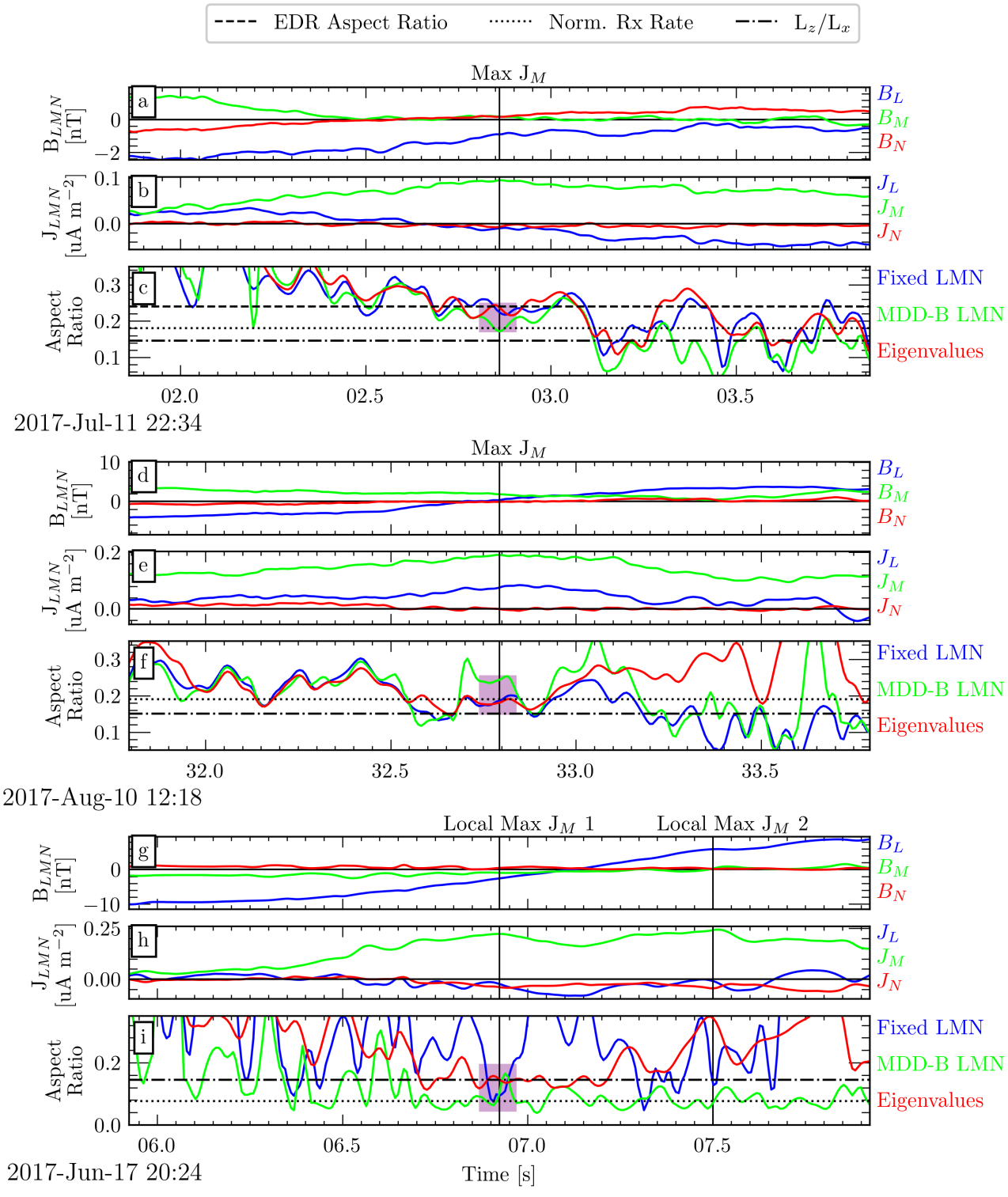
EDR Aspect Ratio
Norm. Rx Rate
L_z/L_x
Max J_M
a
b
c
B_{LMN} [nT]
J_{LMN} [uA m^{-2}]
Aspect Ratio
B_L
B_M
B_N
J_L
J_M
J_N
Fixed LMN
MDD-B LMN
Eigenvalues
02.0
02.5
03.0
03.5
2017-Jul-11 22:34
Max J_M
d
e
f
32.0
32.5
33.0
33.5
2017-Aug-10 12:18
Local Max J_M 1
Local Max J_M 2
g
h
i
06.0
06.5
07.0
07.5
2017-Jun-17 20:24
Time [s]